JOURNAL OF PROPULSION AND POWER
Vol. 11, No. 5, September–October 1995

Technical Notes

TECHNICAL NOTES are short manuscripts describing new developments or important results of a preliminary nature. These Notes cannot exceed 6 manuscript pages and 3 figures; a page of text may be substituted for a figure and vice versa. After informal review by the editors, they may be published within a few months of the date of receipt. Style requirements are the same as for regular contributions (see inside back cover).

Function Approximation Approach to Anomaly Detection in Propulsion System Test Data

Bruce A. Whitehead*
University of Tennessee Space Institute, Tullahoma, Tennessee 37388-8897
and
W. Andes Hoyt†
ERC, Inc., Tullahoma, Tennessee 37388

Nomenclature

f = function to be approximated by the neural network
g = Gaussian bar basis function
nM = number of basis functions per input

N = number of inputs to the neural network
x = vector of inputs to the neural network
μ = basis function center
σ = basis function width

Subscripts
j = which basis function
k = component of input vector

Introduction

A FULLY instrumented ground test of a propulsion system typically generates a very large quantity of data. We propose a screening system to identify the relatively small volume of data that is unusual or anomalous in some way. Limited and expensive human analysis can then focus on this small volume of unusual data.

A liquid-fueled rocket engine, such as the Space Shuttle Main Engine (SSME), is a system with physical and informational interfaces to other systems. A relatively clean interface is defined by a boundary drawn around the engine controller and the system it controls (valves, turbopumps, etc.). The external influences that affect the state of the system include the informational interface of commands given to the controller, as well as physical interfaces such as the fuel inlet, the oxidizer inlet, and the venting and repressurization interfaces to both the fuel and oxidizer tanks. The following 14 measurements at these interfaces, together with 4 turbopump configuration variables, form the 18 inputs to our neural network model:

1) Parameter 287, commanded main combustion chamber pressure, psi
2) Parameter 819, engine fuel inlet pressure no. 2, psi
3) Parameter 821, engine fuel inlet pressure no. 1, psi
4) Parameter 827, engine fuel inlet pressure no. 3, psi
5) Parameter 830, fuel bleed interface pressure, psi
6) Parameter 835, fuel pressurization interface pressure, psi
7) Parameter 836, fuel pressurization venturi inlet pressure, psi
8) Parameter 837, fuel pressurization venturi delta pressure, psi
9) Parameter 858, engine oxidizer inlet pressure no. 2, psi
10) Parameter 859, engine oxidizer inlet pressure no. 1, psi
11) Parameter 860, engine oxidizer inlet pressure no. 3, psi
12) Parameter 878, heat exchanger interface pressure, psi
13) Parameter 881, heat exchanger venturi inlet pressure, psi
14) Parameter 883, heat exchanger venturi delta pressure, psi
15) Installed low-pressure fuel turbopump (2109R6 or 2218R2)
16) Installed high-pressure fuel turbopump (4604, 4406R1, or 6108)
17) Installed low-pressure oxidizer turbopump (2106R2 or 2118)
18) Installed high-pressure oxidizer turbopump (0810, 2030, 2315R1, 4108, or 9409)

Under nominal steady-state operating conditions the behavior of the engine is, in principle, determined by what transpires at these interfaces. To the extent that the SSME is a deterministic system, there would exist some function f that predicts the nominal steady-state value of any desired engine parameter from measurements at all interfaces at the system boundary, e.g., from the measurements listed above. A neural network can be trained to approximate f. Since this study attempts to predict only steady-state parameter values, transients due to SSME power-level changes and to fuel and oxidizer repressurization were automatically removed from the time series inputs to the neural network.

Our approach to identifying anomalous behavior is to train the neural network not to classify anomalies, but to predict nominal values of engine parameters. Representative anomalous data is not needed for training because the neural network is not trying to predict anything about anomalies. Rather, the neural network is trying to predict, as accurately as possible, the nominal steady-state value of each engine parameter under the given interface conditions at each point in time. The detection of anomalies depends upon surrounding the neural network's predictions with a nominal confidence interval. To achieve an acceptably low false alarm rate, the confidence interval is set to five standard deviations above and below the predicted value. Measured values falling outside this confidence interval are flagged as anomalous.

Received Feb. 8, 1993; presented as Paper 93-1776 at the AIAA/SAE/ASME/ASEE 29th Joint Propulsion Conference and Exhibit, Monterey, CA, June 28–30, 1993; revision received Oct. 21, 1994; accepted for publication Nov. 22, 1994.

*Associate Professor of Computer Science, M/S 21. Member AIAA.
†Project Manager, P.O. Box 417. Member AIAA.

Method

Three function-approximation techniques were investigated: 1) a novel neural network architecture based on Gaussian bar basis functions, 2) a standard backpropagation neural network,[1] and 3) standard linear regression. In contrast to 3, 1 and 2 are nonlinear function approximation techniques. The Gaussian bar basis function architecture was investigated because of two difficulties in the application of backpropagation to real problems: the slowness of the gradient descent optimization when multiple layers are involved, and the possibility of getting stuck on a local minimum.

To model a function f with N input variables, we propose a set of semilocal Gaussian bar basis functions[2,3] spaced equally along each dimension of the input data. The set of possible values of each input variable x_k is covered by a set of M basis functions

$$g_{jk}(x_k) = \exp\left[-\frac{(x_k - \mu_{jk})^2}{2\sigma_j^2}\right], \quad j = 1, \ldots, M \quad (1)$$

where the M centers $\mu_{1k}, \ldots, \mu_{Mk}$ are equally spaced along the interval of x_k covered by the training data. Altogether, there are accordingly MN basis functions g_{jk}, $j = 1, \ldots, M$, and $k = 1, \ldots, N$. This proposed Gaussian bar basis function network approximates a real-valued function $f(x)$ as a linear combination of these basis functions using a gradient descent learning rule.[4]

NASA engineers selected two tasks for our study.

1) Detect anomalies in engine parameter 42 for SSME tests 901-671, 901-672, and 901-673.

2) Detect anomalies in engine parameter 221 for SSME tests 902-548, 902-549, and 902-550. The Gaussian bar basis function network was implemented with $M = 60$ and $N = 18$; backpropagation with 1-8, 10, 12, and 16 middle-layer nodes.

Results and Discussion

As expected, the Gaussian bar basis function technique showed more rapid training than backpropagation in both tasks. This result was expected because only a small fraction of the weights are adjusted for each training example.

Figures 1 and 2 show the nominal predictions made by the Gaussian bar basis function neural network for these two SSME tests.

In SSME test 901-672, all three function-approximation techniques correctly identified the anomaly at the right time. This lends support to our hypothesis that nominal behavior of the SSME can be predicted from the external influences crossing the system boundary. The prediction accuracy allows the fluctuation due to the anomaly to be clearly distinguished from the noise fluctuations that nominally arise inside the SSME and due to measurement errors. The anomaly is detected at approximately five times the rms noise level.

In SSME test 902-549, the Gaussian bar basis function network constructed a much tighter confidence interval than the other two techniques, and hence, detected the anomaly at 20 times the rms noise level; linear regression at 4–6 times the rms noise level; and backpropagation at only 2–3 times the rms noise level.

The chief appeal of the function-approximation approach to anomaly detection is that it is not limited to detecting specific, foreseen classes of anomalies, in contrast with most other types of neural network and expert system approaches. Instead, training requires nominal data only, and anomaly detection is based on nominal confidence intervals. Based on the results we have presented, it appears that the function-approximation approach, and its implementation using basis functions, merits more extensive investigation of its practicality for screening large amounts of propulsion system test data. The approach needs to be tested on a larger scale, and it needs to be extended to cover transient as well as steady-state data. Both types of further work are in progress and will be reported at a later date.

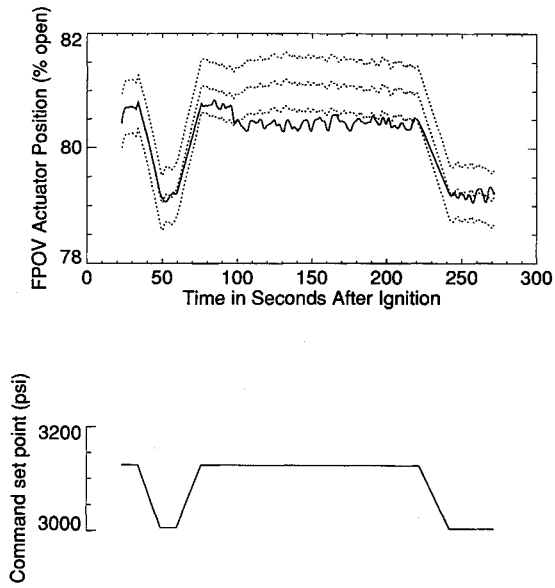

Fig. 1 Neural network screening of data from SSME test 901-672, which was determined by NASA to have an anomaly at 96 s indicated in the fuel preburner oxidizer valve actuator position. The dotted lines show a nominal confidence interval of plus or minus five times the nominal rms prediction error. The middle dotted line is the neural network's prediction. (Sloping segments in the accompanying power-level plot represent transient regions in which no predictions were made. Different steady-state segments are connected by straight lines for visual continuity.) The anomaly is indicated when the measured value of this valve position (solid line) moves outside the nominal confidence interval (bounded by dotted lines).

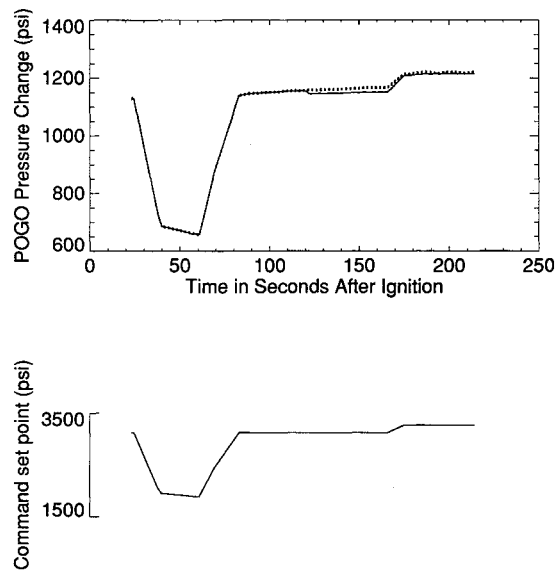

Fig. 2 Neural network screening of data from SSME test 902-549, which was determined by NASA to have an anomaly at 120 s indicated in the pressure change in the POGO surge suppression system. Confidence intervals as in Fig. 1.

Acknowledgments

A portion of this work was supported by NASA Contract NAS8-39184. We thank Timothy Choate, Jo Anne Malone, Michael Whitley, Catherine McLeod, Gary Lyles, Marc Neely, Eric Sander, and Jeff Cornelius for their assistance.

References

[1]Rumelhart, D. E., Hinton, G. E., and Williams, R. J., "Learning Internal Representations by Error Propagation," *Parallel Distributed Processing: Explorations in the Microstructure of Cognition Volume 1: Foundations*, Massachusetts Inst. of Technology Press, Cambridge, MA, 1986, pp. 318–364.

[2]Hartman, E., and Keeler, J. D., "Semi-Local Units for Prediction," *IJCNN-91-Seattle: International Joint Conference on Neural Networks*, Vol. II, IEEE, Piscataway, NJ, 1991, pp. 561–566.

[3]Hartman, E., and Keeler, J. D., "Predicting the Future: Advantages of Semilocal Units," *Neural Computation*, Vol. 3, No. 4, 1991, pp. 566–578.

[4]Widrow, B., and Hoff, M. E., "Adaptive Switching Circuits," *1960 WESCON Convention*, Inst. of Radio Engineers, New York, 1960, pp. 96–104.

Numerical Analysis of Base Flowfield for a Four-Engine Clustered Nozzle Configuration

Ten-See Wang*
NASA Marshall Space Flight Center, Huntsville, Alabama 35812

Introduction

EXCESSIVE base heating has been a problem for many launch vehicles. For certain designs such as the direct dump of turbine exhaust inside and at the lip of the nozzle, the potential burning of the turbine exhaust in the base region can be of great concern. Accurate prediction of the base environment at altitudes is therefore very important during the vehicle design phase. Otherwise, undesirable consequences may occur.

In this study, the turbulent base flowfield of a cold flow experimental investigation[1] for a four-engine clustered nozzle was numerically benchmarked using a pressure-based computational fluid dynamics (CFD) method. This is a necessary step before the benchmarking of hot flow and combustion flow tests can be considered. Since the medium was unheated air, reasonable prediction of the base pressure distribution at high altitude was the main goal. Several physical phenomena pertaining to the multiengine clustered nozzle base flow physics were deduced from the analysis.

Numerical Modeling

The basic equations employed in this study to describe the base flowfield for a four-engine clustered nozzle are the three-dimensional, general-coordinate transport equations. These are equations of continuity, momentum, enthalpy, turbulent kinetic energy, and turbulent kinetic energy dissipation rate. A standard two-equation turbulence model is used to describe the turbulence.

Presented as Paper 93-1923 at the AIAA/SAE/ASME/ASEE 29th Joint Propulsion Conference and Exhibit, Monterey, CA, June 28–30, 1993; received Aug. 6, 1993; revision received Oct. 11, 1994; accepted for publication Nov. 22, 1994.

*Researcher, Computational Fluid Dynamics Branch. Member AIAA.

To solve the system of nonlinear partial differential equations (PDEs), it uses finite difference approximations to establish a system of linearized algebraic equations. An adaptive upwind scheme was employed to approximate the convective terms of the momentum, energy, and continuity equations; the scheme is based on second- and fourth-order central differencing with artificial dissipation. The dissipation terms are constructed such that a fourth-order central and fourth-order damping scheme is activated in smooth regions, and a second-order central and second-order damping scheme is used near shock waves. Viscous fluxes and source terms are discretized using second-order central difference approximation. A pressure-based predictor plus multicorrector solution method is employed so that flow over a wide speed range can be analyzed. The basic idea of this pressure-based method is to perform corrections for the pressure and velocity fields by solving a pressure correction equation so that velocity/pressure coupling is enforced, based on the continuity constraint at the end of each iteration. Details of the present numerical methodology are given in Ref. 2.

Computational Grid Generation

A typical layout of the computational grid is shown in Fig. 1. The four nozzles, which are conical with a cylindrical external shell, are equally spaced on a circular base.[1] Due to the symmetrical nature of the flowfield, only one-eighth of this layout is generated and used for the actual calculation. The two sides of the pie-shaped grid, as shown in Fig. 1, are the symmetry planes. Two grid zones were created. The first zone started at the base and included the nozzle and the plume region. The second zone (the outer shell) comprises the ambient air and a portion of the expanded plume.

Three algebraic grids were generated for the purpose of this report. The difference among these three grids can be visualized by taking a section from the nozzle symmetry plane that lies in between the nozzle centerline and model centerline, as shown in Fig. 1. Grid A has 34,030 points, whereas the grid density for grid B and C is 113,202 points. An ambient-to-total-pressure ratio, $P_a/P_0 = 39 \times 10^{-4}$, is chosen as the nozzle operating condition. The grid lines near the nozzle lip of grid C are slanted to match the Prandtl–Meyer expansion.

Boundary Conditions

To start the calculation, an axisymmetric nozzle flow solution at the prescribed nozzle condition was carried out in a separate manner. The converged flow solution was then mapped to a three-dimensional nozzle flowfield. The nozzle lip, nozzle outer wall, and the base were specified as no-slip wall boundaries. The exit planes of zones 1 and 2, the outer surface (shell) of zone 2, and the inlet plane of zone 2 (flush with the base shield plane) were specified as exit boundaries. In addition, a fixed (ambient) pressure was imposed on the inlet plane of zone 2 in order to obtain a unique solution for the corresponding altitude. Flow properties at the wall, symmetry plane, and exit boundary were extrapolated from those of the interior domain. A tangency condition was applied at the symmetry planes.

Results and Discussion

At this ambient pressure, which corresponds to an altitude of 91,800 ft, the four exhaust plumes have interacted and a reverse jet is formed. The reverse jet impinges on the center of the base and spreads out, forming a wall jet. This wall jet may be choked once the ambient pressure is lower than a critical limit. A comparison of the computed radial base pressure profiles with data is shown in Fig. 2. In general, the peak pressure occurred at the base center and the base pressure decreased as the radial distance from the center of heat shield increased.